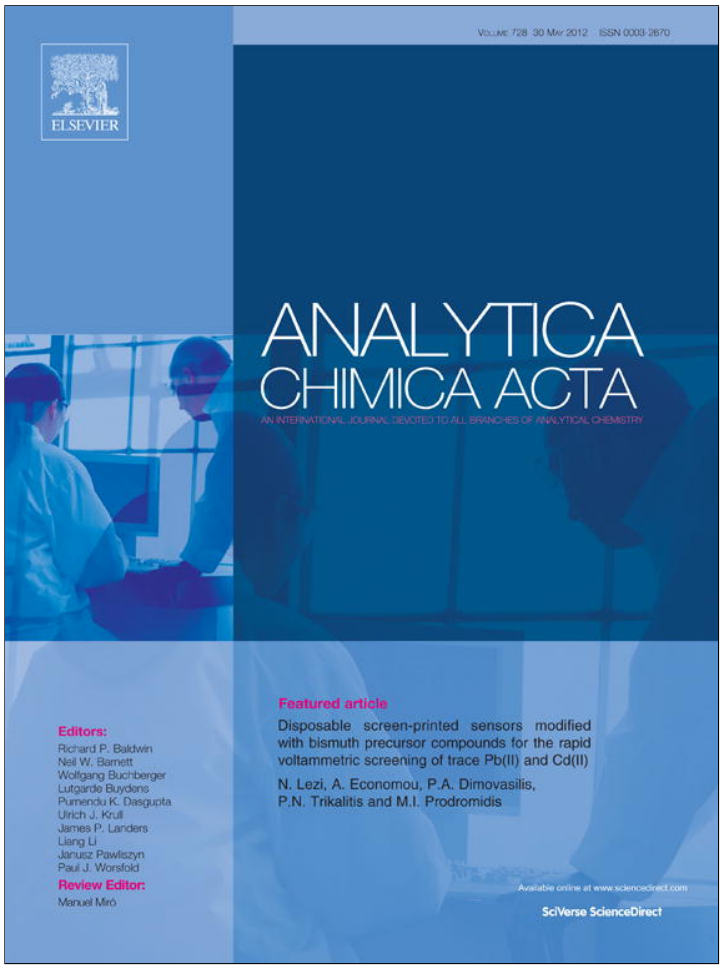

Analytica Chimica Acta 728 (2012) 77–85

Contents lists available at SciVerse ScienceDirect

Analytica Chimica Acta

journal homepage: www.elsevier.com/locate/aca

A ratiometric fluorescence sensor for Be^{2+} based on Beryllon II/layered double hydroxide ultrathin films

Xiaolan Ji, Wenying Shi, Shitong Zhang, Min Wei*, David G. Evans, Xue Duan

State Key Laboratory of Chemical Resource Engineering, Beijing University of Chemical Technology, Beijing 100029, PR China

ARTICLE INFO

Article history:
Received 13 December 2011
Received in revised form 14 February 2012
Accepted 1 April 2012
Available online 7 April 2012

Keywords:
Beryllon II
Layered double hydroxide
Ratiometric fluorescence sensor
Ultrathin film
Beryllium

ABSTRACT

A ratiometric fluorescence sensor for Be^{2+} has been fabricated *via* alternate assembly of 2-(3,6-disulfo-8-hydroxynaphthylazo)-1,8-dihydroxynaphthalene-3,6-disulfonate (Beryllon II) and MgAl-LDH nanosheets on quartz substrates using the layer-by-layer (LBL) deposition technique. UV–vis absorption and the fluorescence emission spectroscopy indicate a stepwise and regular growth of the Beryllon II/LDH UTFs upon increasing deposition cycle. The film of Beryllon II/LDH possesses a periodic layered structure perpendicular to the substrate revealed by X-ray diffraction and scanning electron microscopy. Atomic force microscopy images show that the film surface is continuous and uniform. The Beryllon II/LDH UTFs display ratiometric fluorescence response for Be^{2+} with a linear response range in 1.0×10^{-7}–1.9×10^{-6} mol L^{-1} and a detection limit of 4.2×10^{-9} mol L^{-1}. Furthermore, the ratiometric sensor exhibits good repeatability, high stability (thermal, storage and mechanical) as well as excellent selectivity toward Be^{2+}. XPS and Raman measurements demonstrate that the specific response of the sensor is attributed to the coordination between Be^{2+} and Beryllon II in the UTF. The Beryllon II/LDH UTFs in this work can be potentially used as a chemosensor for the detection of Be^{2+} in the environmental and biomedical field.

1. Introduction

Recently, the existence of beryllium in soil, water and food has attracted much attention due to its high toxicity and debated carcinogenicity. Therefore, detection of this element is of considerable significance in their disposal sites as well as in the industry using beryllium products [1,2]. The determination of beryllium has been generally carried out based on atomic absorption spectrometry [3–5], fluorometry [6,7], voltammetry [8–10] and high-performance liquid chromatography (HPLC) [11]. Fluorescence spectroscopy is a powerful method to detect ions and neutral molecules because of its high sensitivity, selectivity, fast-response and low cost [12–17]. However, a key disadvantage of fluorescence determination is that the fluorescence indicators generally suffer from changeable fluorescence intensity upon the agitation of external environment (pH, polarity, temperature, photobleaching). Compared with intensity-based systems, ratiometric fluorescence sensors are preferred in bioimaging applications because this measurement involves the change of intensity ratio of absorption or emission at two wavelengths, which effectively eliminates most or all interferences from environment and thus increases the selectivity and sensitivity [18–25]. Up to now, considerable efforts have been focused on the development of fluorescence sensors for Zn^{2+} [26–30], Ag^{+} [31–33], and Pb^{2+} [34,35] *etc.*, based on the ratiometric fluorescence method.

Organic fluorescence indicators are normally prone to be thermally or optically unstable, which limits their practical application. One effective solution to this problem is the incorporation of indicator molecules into solid supports. Recently, the fabrication of organic chromophore–inorganic matrix composite materials has attracted much attention owing to their novel functionalities which are not present in the individual components [36–40]. Layered double hydroxides (LDHs) are one type of 2D inorganic materials whose general formula can be expressed as $[M^{II}_{1-x}M^{III}_{x}(OH)_2]^{z+}A^{n-}_{z/n}{\cdot}yH_2O$, where M^{II} and M^{III} are divalent and trivalent metals respectively; A^{n-} is the anion to compensate for the positive charge of the hydroxide layers [41,42]. LDH materials have been widely used in the fields of catalysis [43,44], separation process [45] and drug delivery [46–48] based on their specific intercalation property. Recently, the delamination of LDH into nanosheets as building blocks and preparation of inorganic/organic fluorophore ultrathin films (UTFs) have been reported [49,50]. This inspires us to challenge the goal of fabricating fluorescence chemosensors *via* alternate assembly of positively charged LDH nanosheets and negatively charged fluorophore indicators with the layer-by-layer (LBL) technique. The resulting UTFs

* Corresponding author. Tel.: +86 10 64412131; fax: +86 10 64425385.
E-mail addresses: weimin@mail.buct.edu.cn, weimin-hewei@163.com (M. Wei).

0003-2670/$ – see front matter © 2012 Elsevier B.V. All rights reserved.
http://dx.doi.org/10.1016/j.aca.2012.04.001

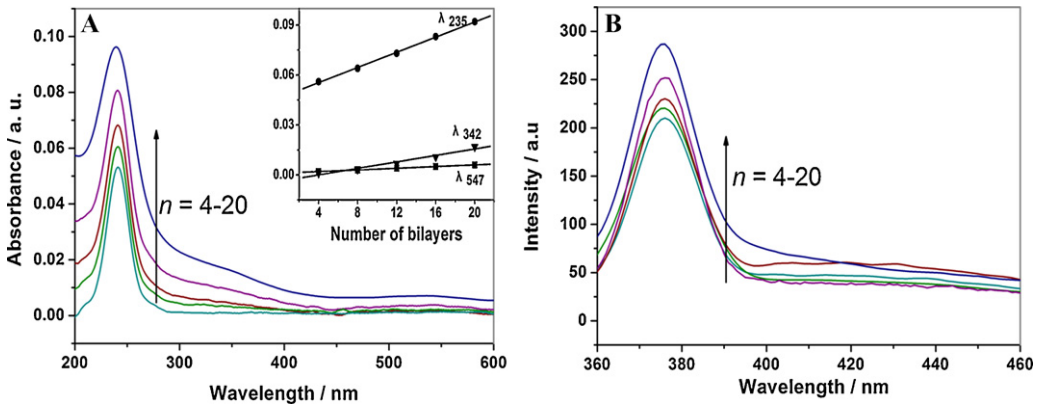

Fig. 1. (A) UV–vis absorption spectra of the (Beryllon II/LDH)$_n$ UTFs (n = 4–20) (inset: plots of the absorbance at 235, 342 and 547 nm *vs.* n); (B) the emission spectra of the (Beryllon II/LDH)$_n$ UTFs (n = 4–20).

would exhibit the following advantages: firstly, the LDH matrix would enhance the optical and thermal stability of the chromophore due to the ordered stacking of the LDH nanosheets; secondly, the molecular level control of the assembly will result in a high dispersion of fluorophore molecules with uniform orientation, which can suppress aggregation and reduce fluorescence quenching effectively.

2-(3,6-Disulfo-8-hydroxynaphthylazo)-1,8-dihydroxynaphthalene-3,6-disulfonate (Beryllon II) is one of the most promising indicators in chemical sensor application, which has been used as a chromogenic reagent to determine cations and proteins under different conditions [51–54]. Its absorption and fluorescence emission strongly depend on pH value owing to the presence of cationic, neutral and anionic forms in aqueous solution. In this work, fluorophore Beryllon II and MgAl-LDH nanosheets were alternately assembled on quartz substrates using the LBL method, which was demonstrated as a ratiometric fluorescence chemosensor for Be^{2+}. The Beryllon II/LDH UTF chemosensor shows a linear response range (1.0×10^{-7}–1.9×10^{-6} mol L^{-1}) and a low detection limit (4.2×10^{-9} mol L^{-1}) at the optimal working pH (11.0). In addition, its thermal- and storage stability, repeatability as well as excellent selectivity toward Be^{2+} have been demonstrated. The regeneration of the chemosensor was also achieved, which induced reversible changes in surface morphology and fluorescence anisotropy. Therefore, the strategy in this work provides a successfully paradigm for the fabrication of highly oriented luminescence UTFs based on an organic indicator immobilized within an inorganic matrix, which can be potentially applied as chemosensors in environmental and biological fields.

2. Experimental

2.1. Materials

2-(3,6-Disulfo-8-hydroxynaphthylazo)-1,8-dihydroxynaphthalene-3,6-disulfonate (Beryllon II, biochemistry grade) was purchased from Sigma–Aldrich Company. Analytical grade chemicals including $Mg(NO_3)_2{\cdot}6H_2O$, $Al(NO_3)_3{\cdot}9H_2O$, NaOH, $Ca(NO_3)_2$, $Cd(NO_3)_2$, $NaNO_3$, $Hg(NO_3)_2$, $Co(NO_3)_2$, $Cu(NO_3)_2$, $Zn(NO_3)_2$, NH_4VO_3, $Pb(NO_3)_2$, $Fe(NO_3)_3$, KNO_3, $Mn(NO_3)_2$, $Ni(NO_3)_2$, $BeSO_4$ and KF were used without further purification. The deionized and decarbonated water was used in all the experimental processes.

2.2. Fabrication of the (Beryllon II/LDH)$_n$ UTFs

The Mg_2Al–NO_3 LDH precursor was synthesized by a hydrothermal method reported previously [55] and its XRD pattern is shown in Fig. S1. A 0.1 g of Mg_2Al–NO_3 LDH was shaken in 100 mL of formamide solution for 24 h to obtain a colloidal suspension of exfoliated Mg_2Al–NO_3 LDH nanosheets. The quartz glass substrate was cleaned in concentrated NH_3/30% H_2O_2 (7:3, v/v) and concentrated H_2SO_4 for 30 min each. After each procedure, the quartz substrate was rinsed and washed thoroughly with deionized water. The substrate was dipped in a colloidal suspension (0.1 g mL^{-1}) of LDH nanosheets for 10 min followed by washing thoroughly, and then the substrate was treated with a 100 mL of Beryllon II aqueous solution (0.025 wt%) for another 10 min followed by washing. Multilayer films of (Beryllon II/LDH)$_n$ were fabricated by alternate deposition of LDH nanosheets suspension and Beryllon II solution for n cycles. The resulting films were dried with a nitrogen gas flow at 25 °C for 2 min.

2.3. The response of the UTF toward Be^{2+}

The Be^{2+} solutions with different concentrations were prepared by dissolving $BeSO_4$ in deionized water. The fluorescence chemosensor was immersed into a quartz cell with $BeSO_4$ solution, and its response was recorded by a RF-5301PC fluorophotometer with a liquid holder.

2.4. Characterization techniques

The UV–vis absorption spectra were collected in the range from 280 to 550 nm on a Shimadzu T-9201 spectrophotometer, with the slit width of 1.0 nm. The fluorescence spectra were performed on a RF-5301PC fluorospectrophotometer with the excitation wavelength of 333 nm. The fluorescence emission spectra range in 350–600 nm, and both the excitation and emission slits were set to 5 nm. Steady-state polarized photoluminescence measurements of the Beryllon II/LDH UTFs were recorded with an Edinburgh Instruments' FLS 920 fluorospectrophotometer. X-ray diffraction patterns (XRD) were recorded using a Rigaku 2500 VB2 + PC diffractometer under the conditions: 40 kV, 50 mA, Cu Kα radiation (λ = 0.154 nm) step-scanned with a scanning rate of 0.5° min^{-1}, and a 2θ angle ranging from 0.5° to 10°. The morphology of thin films was investigated by using a scanning electron microscope (SEM ZEISS), and the accelerating voltage applied was 20 kV. The surface roughness and thickness data were obtained by using the atomic force microscopy (AFM) software (Digital Instruments,

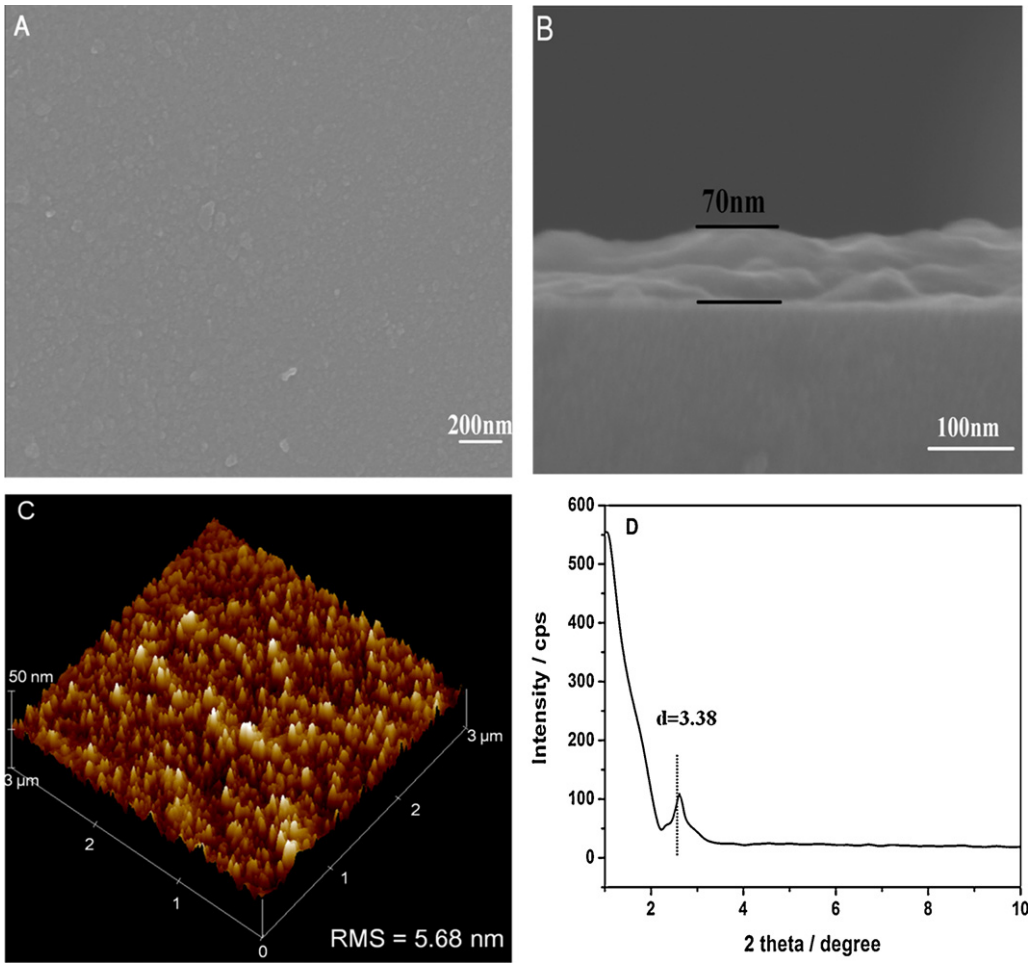

Fig. 2. (A) Top-view of SEM image, (B) side-view of SEM image, (C) tapping-mode AFM image and (D) XRD pattern of the (Beryllon II/LDH)$_{20}$ UTF.

version 6.12). Be elemental analysis was performed by inductively coupled plasma atomic emission spectroscopy (ICP-AES) with a Shimadzu ICPS-7500 instrument. X-ray photoelectron spectroscopy (XPS) measurement was performed with monochromatized A1 Kα exciting X-radiation (PHI Quantera SXM). The Raman spectra were obtained with 785 nm of excitation by using a confocal Raman microspectrometer (Renishaw Instruments Co. Ltd., RM2000) in the range 1000–2500 cm^{-1}.

3. Results and discussion

3.1. Characterization of the Beryllon II/LDH UTFs

3.1.1. Assembly of the UTFs

The UV–vis absorption spectra measurements for the (Beryllon II/LDH)$_n$ UTFs with various deposition cycles during the assembly are shown in Fig. 1A. The absorption bands of (Beryllon II/LDH)$_n$ UTFs at ~235 nm, 342 nm (π–π* transition) and 547 nm (*n*–π* transition) correlate linearly with the bilayer number *n*, demonstrating an ordered and regular film growth procedure, which was further confirmed by the gradual color enhancement with the increase of bilayer number (Fig. S2). Compared with the pristine Beryllon II solution sample (Fig. S3A), the absorption bands of the (Beryllon II/LDH)$_n$ UTFs at ~342 and 547 nm become unresolved, which may be attributed to the electrostatic interaction between Beryllon II anion and LDH nanosheets. The fluorescence emission peak of the (Beryllon II/LDH)$_n$ UTFs at 375 nm presents consistent enhancement with the increase of *n* (Fig. 1B). Compared with Beryllon II solution sample (Fig. S3B), the emission peak of the (Beryllon II/LDH)$_n$ UTFs shows a blue shift (from 420 nm to 375 nm) due to the change in microenvironment of interlayer Beryllon II. The LDH gallery offers a rigid and confined microenvironment for the guest molecule, which leads to a decrease in the rotation freedom of

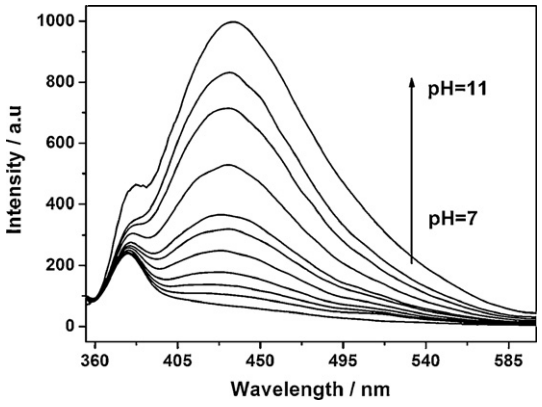

Fig. 3. Emission spectra of the (Beryllon II/LDH)$_{20}$ UTF at different pH values (293 K, λ_{ex} = 333 nm).

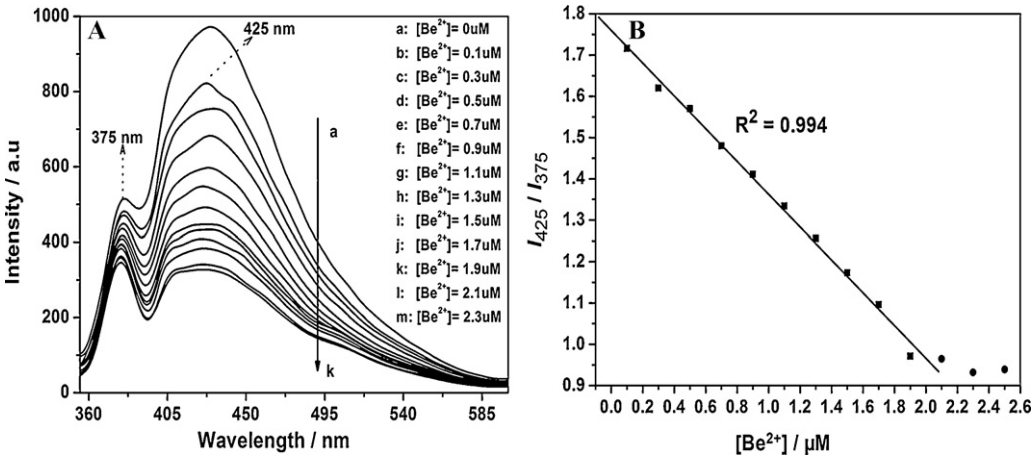

Fig. 4. (A) Emission spectra of the (Beryllon II/LDH)$_{20}$ UTF upon increasing Be^{2+} concentration at pH = 11 (293 K; λ_{ex} = 333 nm); (B) Be^{2+} titration curve of the chemosensor for emission ratio at 425–375 nm (I_{425}/I_{375}).

Beryllon II moiety and the resulting blue shift of emission [56–58]. The deposition process of the (Beryllon II/LDH)$_n$ UTF can also be observed from its side view of SEM images with approximately linear increase (from 28 to 70 nm) upon increasing the bilayer number (n = 8–20), which confirms that the UTFs present uniform and periodic layered structure (Fig. S4).

3.1.2. Structural and morphological characterization

A typical top view of SEM image for the (Beryllon II/LDH)$_{20}$ UTF shows that the film surface is microscopically continuous and smooth (Fig. 2A). The top view of SEM images for the (Beryllon II/LDH)$_n$ UTFs reveal that both the homogeneity and surface coverage of the UTFs increase with the enhancement of bilayer number (Fig. S5). The thickness of the (Beryllon II/LDH)$_{20}$ UTF of ~70 nm can be estimated by observing its side-view SEM image (Fig. 2B), from which it can be estimated that the thickness of one bilayer unit (Beryllon II/LDH)$_1$ is ~3.50 nm. The atomic force microscopy (AFM) image reveals that the film surface is smooth, with a root-mean-square roughness of 5.68 nm (Fig. 2C). XRD pattern (Fig. 2D) exhibits a Bragg peak at $2\theta = 2.61^\circ$, indicating that the UTFs present an orderly periodic structure in the normal direction of the film with a repeating distance of 3.38 nm, which is approximately consistent with the thickness augment per deposited cycle observed by SEM (3.50 nm). Moreover, this is also in agreement with the ideal double-layer model of the Beryllon II/LDH structure with the thickness of ~0.48 nm for one LDH monolayer and 1.56 nm for each extended chain configuration of Beryllon II (Fig. S6).

3.2. The (Beryllon II/LDH)$_{20}$ UTFs as a ratiometric fluorescence chemosensor for Be^{2+}

3.2.1. The response of (Beryllon II/LDH)$_n$ UTFs to pH

The fluorescence emission spectra for the (Beryllon II/LDH)$_{20}$ UTFs at different pH values are shown in Fig. 3. The emission spectrum of the UTF displays a band at 375 nm at pH = 7 (293 K, λ_{ex} = 333 nm); a new emission band at 425 nm is observed and both intensities of the two bands increase along with the enhancement of pH value from 7 up to 11. Beryllon II displays a complex pH-dependent equilibrium resulting from its various ionic forms (Fig. S7) [54]. The changes in relative intensity of the two emission

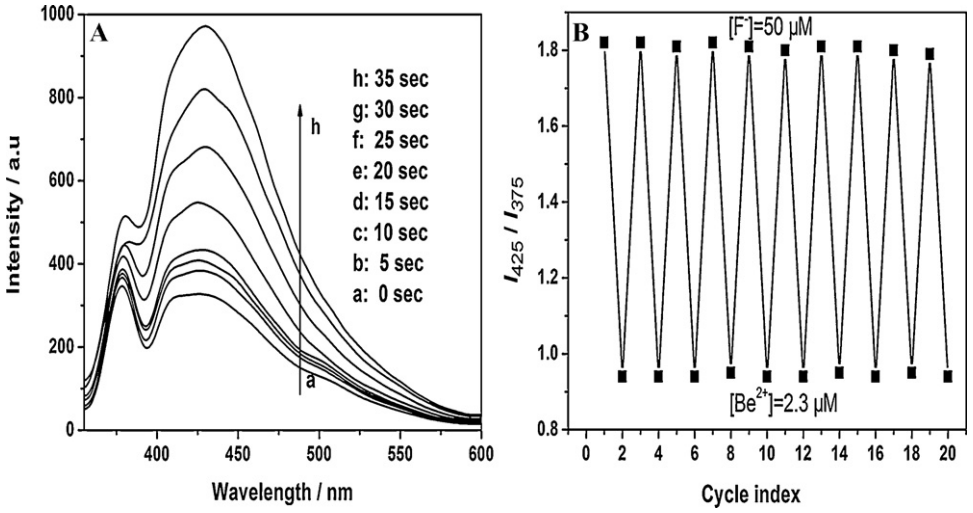

Fig. 5. (A) Emission spectra of the quenched chemosensor in KF (50 μM) as a function of time; (B) the reversibility of the chemosensor recorded by alternate measurement in two solutions of Be^{2+} and KF respectively.

Table 1
Determination of Be^{2+} in the tap and lake water.

Sample	Number	Be^{2+} added (mol L^{-1})	Be^{2+} found (mol L^{-1}) (mean[a] ± S.D.[b])	Recovery (%)
Lake water	No. 1	2.0×10^{-7}	$(2.05 \pm 0.20) \times 10^{-7}$	102.5
	No. 2	5.0×10^{-7}	$(5.06 \pm 0.11) \times 10^{-7}$	101.2
	No. 3	1.0×10^{-6}	$(0.98 \pm 0.17) \times 10^{-6}$	98.0
Tap water	No. 1	2.0×10^{-7}	$(2.02 \pm 0.13) \times 10^{-7}$	101.0
	No. 2	5.0×10^{-7}	$(4.96 \pm 0.15) \times 10^{-7}$	99.2
	No. 3	1.0×10^{-6}	$(1.03 \pm 0.19) \times 10^{-6}$	103.0

[a] Mean of three determinations.
[b] Standard deviation.

peaks are due to the equilibrium transition between different fluorescence forms of Beryllon II in the gallery of LDH. As far as the fluorescence sensitivity is concerned, the (Beryllon II/LDH)$_n$ UTFs were studied at pH = 11 in the following study. Fig. S8A shows the fluorescence intensity of the (Beryllon II/LDH)$_n$ UTFs (n = 4–24) at pH = 11, from which the (Beryllon II/LDH)$_{20}$ UTF displays the strongest fluorescence intensity at 425 nm as well as the largest emission ratio (I_{425}/I_{375}). Therefore, the (Beryllon II/LDH)$_{20}$ UTF sample was chosen in the next section.

3.2.2. The response of the (Beryllon II/LDH)$_{20}$ UTF toward Be^{2+}

In the presence of Be^{2+}, the fluorescence emission spectrum of the (Beryllon II/LDH)$_{20}$ UTF exhibits a significant decrease in the intensity both at 425 nm and 375 nm (Fig. 4A). This indicates the (Beryllon II/LDH)$_{20}$ UTF can be used as a sensitive ratiometric probe toward Be^{2+}. The emission ratio of the (Beryllon II/LDH)$_{20}$ UTF at 425–375 nm (I_{425}/I_{375}) decreases linearly from 1.716 to 0.971 as the concentration of Be^{2+} increases from 0.1 to 1.9 μM, with the following linear regression equation: $I_{425}/I_{375} = 1.757 - 0.414c$ (μM), $r^2 = 0.994$ (Fig. 4B). The absolute detection limit is 4.2 nM, which meets the maximum contaminant level (MCL) for Be^{2+} detection in drinking water according to United States Environmental Protection Agency (EPA) [59]. Fig. S9 shows emission spectra of the (Beryllon II/LDH)$_{20}$ UTF in Be^{2+} solution as a function of time. The response time was 50 s for the (Beryllon II/LDH)$_{20}$ UTF, which is a key feature for its practical application. The fluorescence response of the UTF to Be^{2+} is probably related to the binding between Beryllon II and Be^{2+} [11], which will be further discussed in the next section.

3.2.3. The regeneration and stability

The regeneration and reversibility is of great importance for chemosensors in practical applications. To realize the regeneration of the chemosensor, the quenched (Beryllon II/LDH)$_{20}$ UTF was immersed into a solution of KF (50 μM), and the fluorescence emission ratio (I_{425}/I_{375}) of the UTF increased gradually and recovered completely after 35 s (Fig. 5A), demonstrating the binding between Beryllon II and Be^{2+} is chemically reversible. A good repeatability of the chemosensor was observed with RSD = 0.51% (KF) and RSD = 0.55% (Be^{2+}) in 20 cycles by alternate immersion into two solutions of Be^{2+} and KF respectively (Fig. 5B). In addition, Fig. S10 displays the TG-DTA curves of the pristine Beryllon II and Beryllon II/LDH composite material respectively, from which it can be observed that the thermal stability of Beryllon II is enhanced greatly upon assembly with the LDH nanosheets. Furthermore, the storage stability test of the chemosensor shows that approximately ~90.2% of its initial fluorescence intensity remained after one month measurement (Fig. S10C). As shown in Fig. S11, no delamination or peeling occurred on cross-cutting the surface of the (Beryllon II/LDH)$_{20}$ UTF, indicating a strong adherence of the film to the substrate. The results above demonstrate that the chemosensor possesses high thermal stability and mechanical stability.

3.2.4. Selectivity

It is a key factor to obtain high selectivity of the chemosensor toward analyte over other competitive species. In order to evaluate the selectivity of the (Beryllon II/LDH)$_{20}$ UTF toward Be^{2+}, the fluorescence emission ratio of the UTF at 425–375 nm in solutions containing Zn^{2+}, Al^{3+}, Co^{2+}, Mg^{2+}, Cd^{2+}, Ca^{2+}, Hg^{2+}, Cu^{2+}, Pb^{2+}, Ni^{2+} and Mn^{2+} was recorded, respectively (Fig. 6). It was found that the response of the UTF to these cations was much lower compared

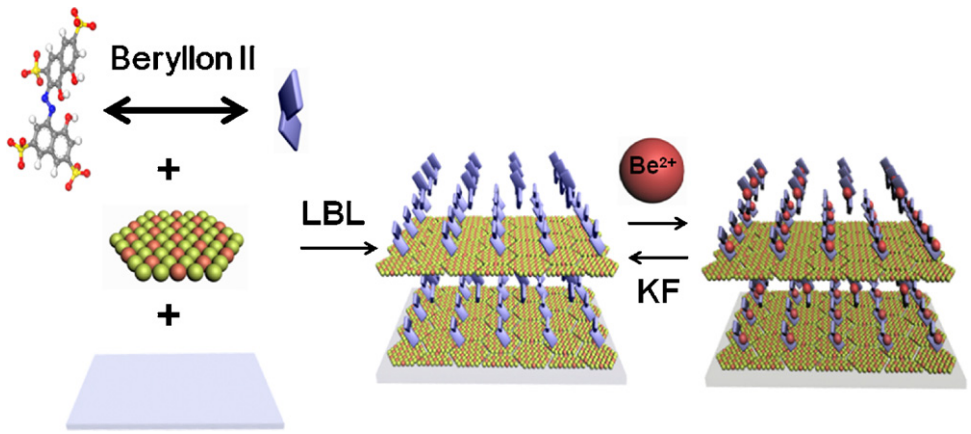

Scheme 1. A schematic representation for the measurement-regeneration cycle of the Beryllon II/LDH UTF (Mg – yellow green, Al – orange, H – white, S – yellow, O – red, N – blue, C – gray, Be – deep red). (For interpretation of the references to color in this scheme legend, the reader is referred to the web version of the article.)

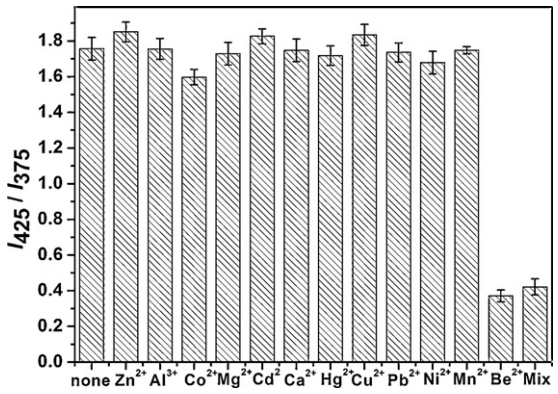

Fig. 6. The fluorescence emission ratio (I_{425}/I_{375}) of the chemosensor induced by indicated metal cations (1 mM each). Mix = a mixed solution containing all the tested cations. Indicated values are means of three measurements with the standard error less than 5%.

with Be^{2+}, and less change in I_{425}/I_{375} for these interferential species (~6%) than Be^{2+} (~79%) was observed. No significant influence on the fluorescence response to Be^{2+} was observed with the presence of a mixture of the above-mentioned metal ions (1 mM each). Be^{2+} mostly coexists with some common cations (Al^{3+}, Fe^{3+}, Mg^{2+}, *etc.*) at the natural abundance level in air–dust samples [60]. Therefore, the artificial surrogate solution for an air–dust sample was studied in this work (Table S1), and the results show that Be^{2+} can be determined with good reproducibility and recovery.

3.2.5. *Determination of Be^{2+} in real water samples*

In order to examine the potential applicability of the ratiometric fluorescence sensor, two samples (tap water and lake water collected from the Weiming lake in the Peking University) were used for the Be^{2+} determination. Each water sample was filtered through a 0.45 μL membrane, and both the samples showed no Be^{2+} by the elemental analysis results based on inductively coupled plasma atomic emission spectrometry (ICP-AES). Therefore, different concentrations of Be^{2+} were respectively added in the water samples and then were measured by the ratiometric fluorescence chemosensor (Table 1). The results of the two samples are satisfactory, indicating that the (Beryllon II/LDH)$_{20}$ UTF can be potentially used as a chemosensor for the detection of Be^{2+} in the environmental field.

3.3. *Studies on the mechanism of measurement-regeneration cycle*

Scheme 1 shows the process of fluorescence quenching and regeneration for the fluorescence chemosensor. A high

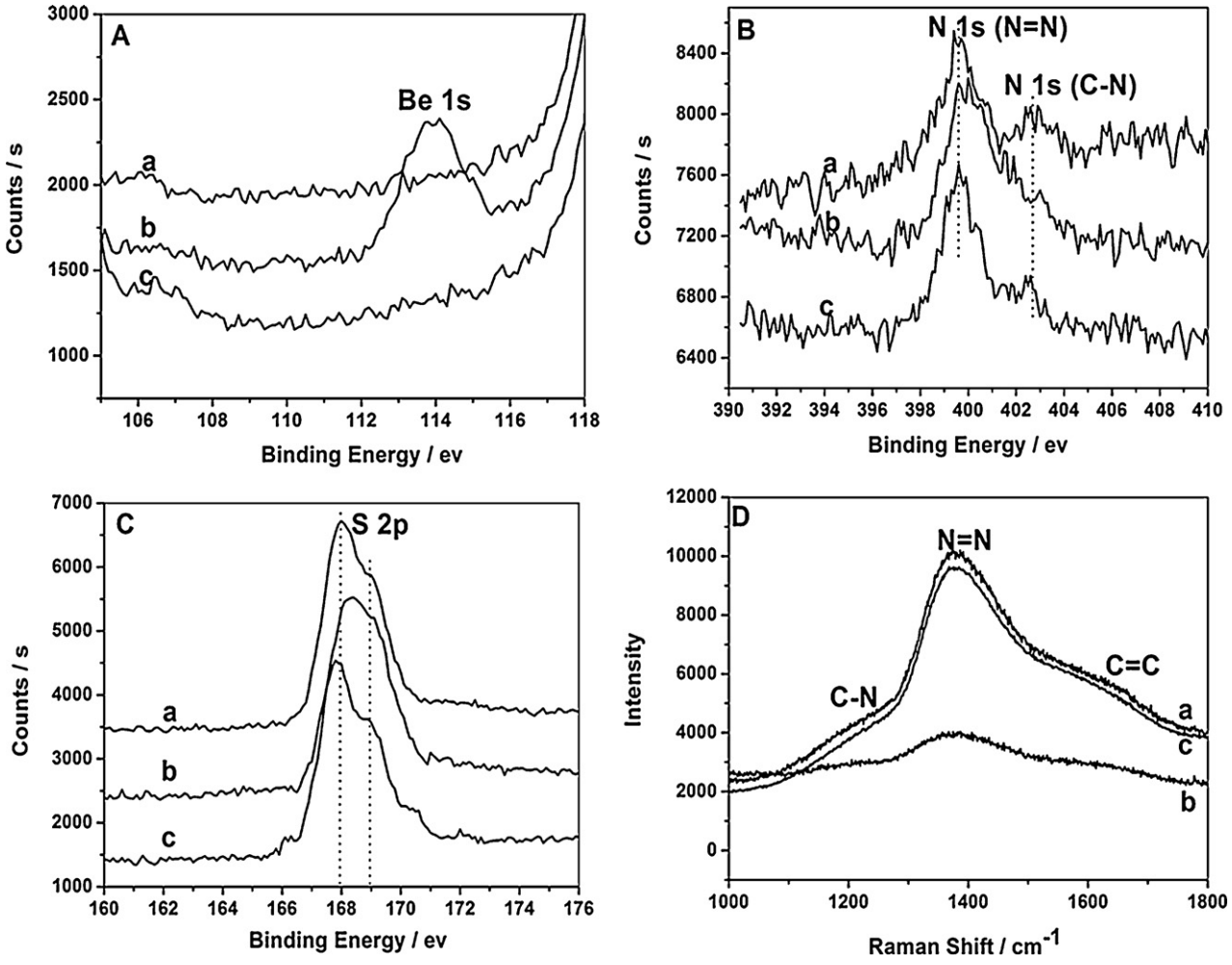

Fig. 7. The XPS spectra of (A) Be 1s (B) N 1s (C) S 2p and (D) Raman spectra: (a) the original (Beryllon II/LDH)$_{20}$ UTF, (b) the UTF after measurement of Be^{2+}, and (c) the regenerated UTF by F^-.

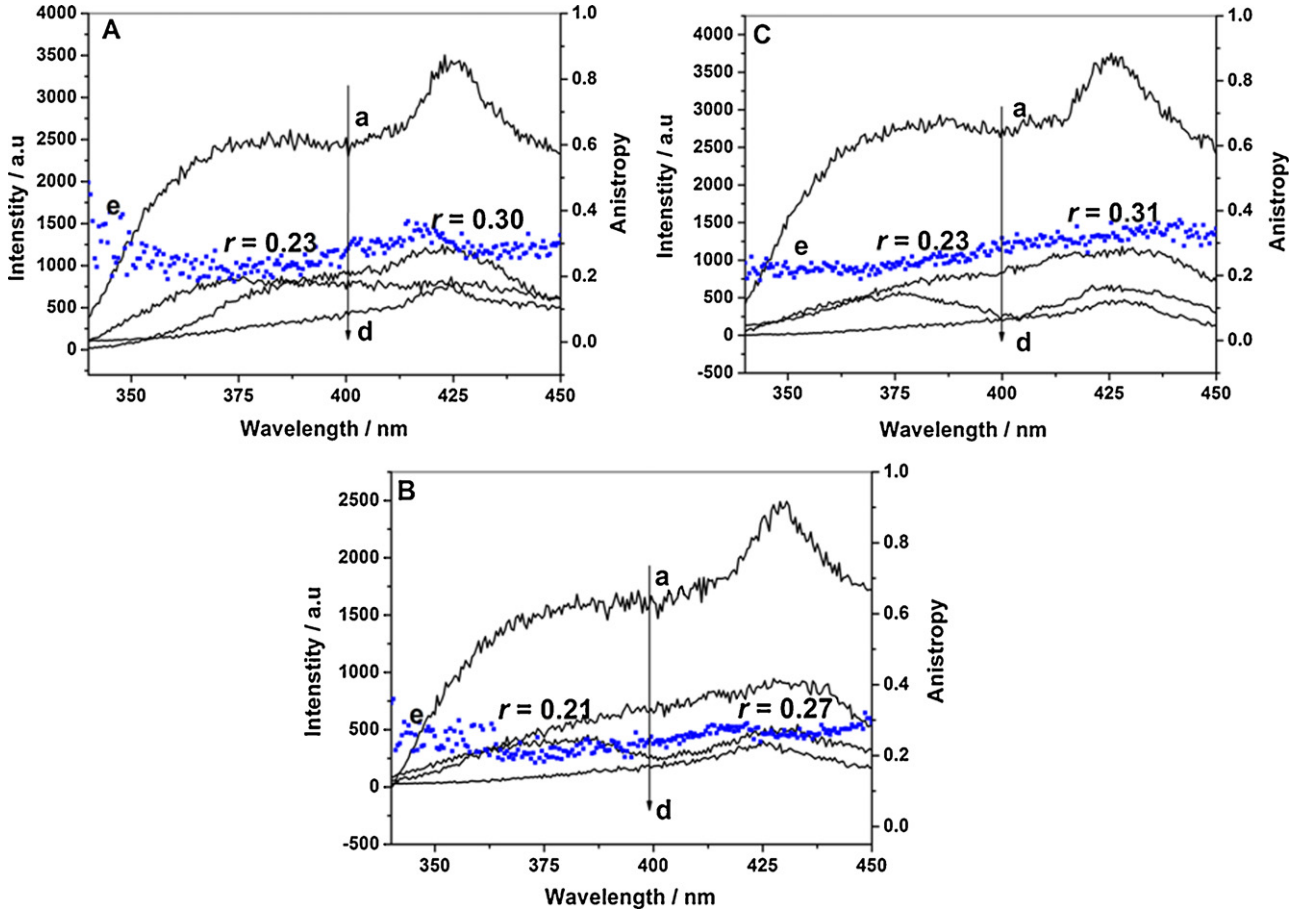

Fig. 8. Photoemission profiles in the (a) VV, (b) VH, (c) HV, (d) HH, (e) polarizations and anisotropy of the sample measured at room temperature (293 K): (A) the original (Beryllon II/LDH)$_{20}$ UTF, (B) the UTF after measurement of Be^{2+}, and (C) the regenerated UTF by F^-.

thermodynamic affinity of Be^{2+} toward typical N and S-chelate ligands and fast metal-to-ligand binding kinetics lead to the complexation of Be^{2+} with Beryllon II in the UTF and the resulting fluorescence quenching; while the regeneration of the quenched UTF was rooted in the complexation of Be^{2+} and F^- owing to the much larger complex constant between F^- and Be^{2+} ($\log K \approx 12.8$) [61] than Beryllon II and Be^{2+} ($\log K \approx 7$ based on the fit result of Stern–Volmer formula, see Fig. S12). This process was supported by the results of XPS and Raman measurements shown in Fig. 7. Compared with the original UTF (Fig. 7A-a), the XPS spectrum after measurement of Be^{2+} (Fig. 7A-b) displays a new peak attributed to Be 1s (113.7 eV), indicating that Be^{2+} was bonded within the UTF *via* the complexation with Beryllon II. The disappearance of Be signal for the regenerated UTF by F^- confirms the removal of Be^{2+} from the UTF (Fig. 7A-c). The XPS peak for N 1s (Fig. 7B-b) of the quenched (Beryllon II/LDH)$_{20}$ UTF (N=N: 400.1 eV; N—C: 402.7 eV) shifted to higher binding energies compared with those of original (N=N: 399.6 eV; N—C: 402.5 eV; Fig. 7B-a) and regenerated one (N=N: 399.7 eV; N—C: 402.4 eV; Fig. 7B-c). A similar shift in the banding energy of S 2p 3/2 was also observed (Fig. 7C), which can be attributed to the reduction of electron density [62]. The results indicate the formation of coordination bond between Be^{2+} and N, S atoms in Beryllon II. This can be further verified by the Raman spectroscopy (Fig. 7D). Compared with the original and regenerated Beryllon II/LDH UTF, the quenched UTF shows significant decrease in the absorption intensity of N=N, C—N and C=C, owing to the complexation between Be^{2+} and N atoms in Beryllon II.

In order to give a further insight into the mechanism of measurement-regeneration cycle, the polarized photoemission spectra of the original (Beryllon II/LDH)$_{20}$ UTF, the quenched and recovered UTF samples were measured and displayed in Fig. 8. One of the most common methods of evaluating fluorescence polarization is the measurement of the anisotropic value *r*, which was fully described by Valeur [63]. The original (Beryllon II/LDH)$_{20}$ UTF (Fig. 8A) shows well-defined fluorescence anisotropy with the anisotropy value (*r*) of 0.23 (375 nm) and 0.30 (425 nm) due to well-oriented arrangement of Beryllon II. However, the anisotropy value decreased to 0.21 (375 nm) and 0.27 (425 nm) respectively after measurement of Be^{2+} (Fig. 8B), indicating the decrease in the conjugacy of Beryllon II owing to its complexation with Be^{2+}. After regeneration by F^- (Fig. 8C), the fluorescence anisotropy value increased to 0.23 (375 nm) and 0.31 (425 nm) respectively as a result of the removal of Be^{2+} from the UTF. In addition, a reversible morphological change was observed by AFM during a measurement-regeneration cycle (Fig. 9). The surface of the original (Beryllon II/LDH)$_{20}$ UTF was smooth with a root-mean square roughness of 6.34 nm (Fig. 9A); while sharp peaks were observed after measurement of Be^{2+} accompanied with a marked increase in RMS roughness (7.47 nm) (Fig. 9B). After regeneration by F^-, a relatively smooth surface was recovered with a RMS roughness of 6.48 nm (Fig. 9C). The reversible changes in both anisotropy and morphology indicate that the embedment/removal of Be^{2+} gives rise to regular variations in orientation and/or stacking of Beryllon II.

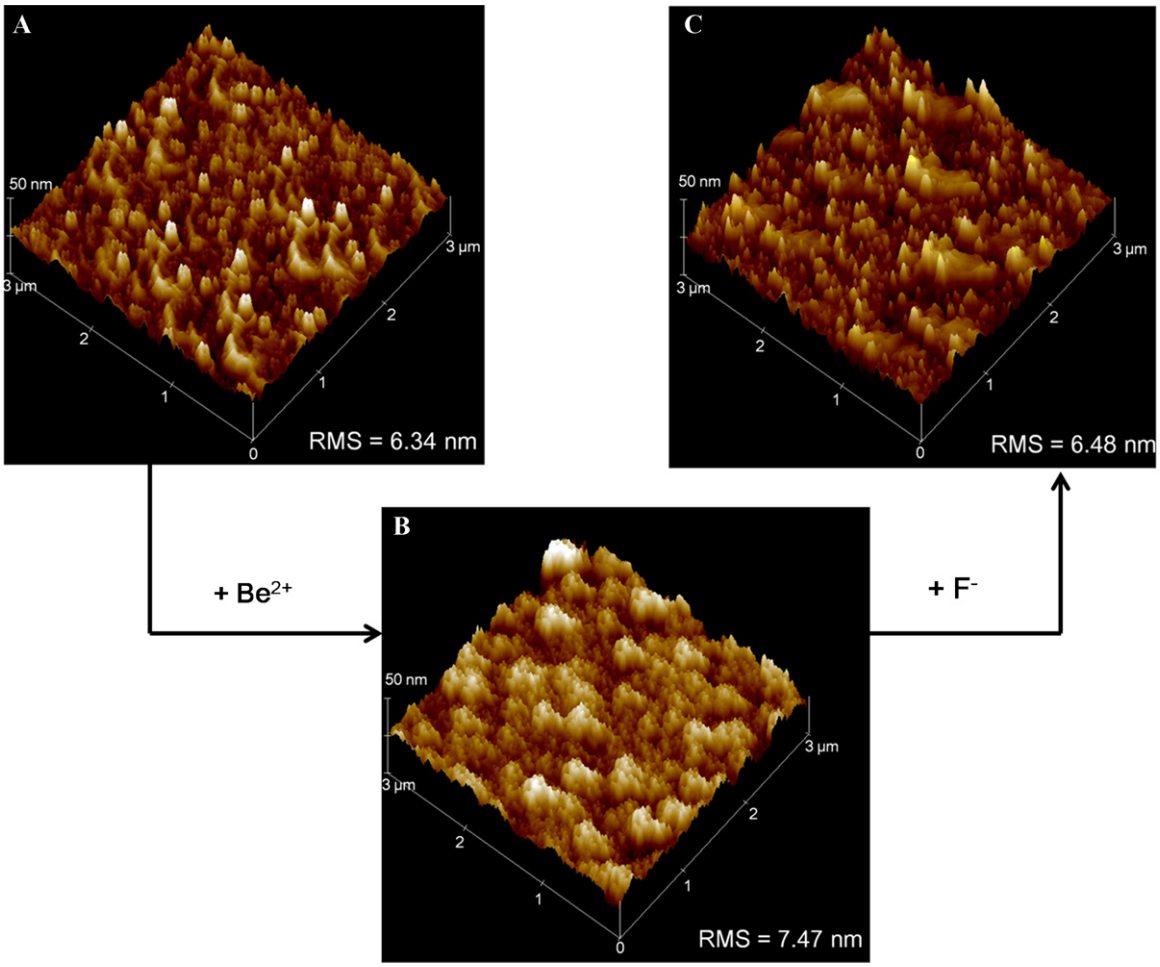

Fig. 9. AFM images of (A) the original (Beryllon II/LDH)$_{20}$ UTF, (B) the UTF after measurement of Be^{2+}, and (C) the regenerated UTF by F^{-}.

4. Conclusions

The fabrication of the ordered (Beryllon II/LDH)$_n$ UTFs by the LBL deposition technique was performed in this work, and their application as a ratiometric fluorescence chemosensor for Be^{2+} was demonstrated. The structural and morphological studies show that the (Beryllon II/LDH)$_n$ UTFs were homogeneous and uniform with long range stacking order in the vertical direction to the substrate. Furthermore, the (Beryllon II/LDH)$_{20}$ UTF displays an excellent ratiometric fluorescence chemosensory behavior for Be^{2+} with a linear response range and a low detection limit. The stability, regeneration as well as selectivity of the sensor guarantee its prospective application. Therefore, this work provides a facile and efficient strategy for the immobilization of organic indicator into an inorganic matrix, which can be potentially used for the detection and measurement of toxic pollutants in the environmental and biomedical fields.

Acknowledgments

This work was supported by the 973 Program (Grant No. 2011CBA00504), the National Natural Science Foundation of China, the 111 Project (Grant No. B07004) and the Collaboration Project from the Beijing Education Committee.

Appendix A. Supplementary data

Supplementary data associated with this article can be found, in the online version, at http://dx.doi.org/10.1016/j.aca.2012.04.001.

References

[1] H. Vainio, J.M. Rice, J. Occup, Environ. Med. 39 (1997) 204–231.
[2] C.W. Jameson, Environ. Health Perspect. 104 (1996) 935–936.
[3] A. Afkhami, T. Madrakian, A.A. Assl, A.A. Sehhat, Anal. Chim. Acta 437 (2001) 17–22.
[4] W.F. Schmidt, F. Dietl, Z. Fresenius, Anal. Chem. 329 (1988) 853–855.
[5] J. Kubova, V. Nevoral, V. Stresko, J. Fresenius, Anal. Chem. 348 (1994) 287–290.
[6] K. Ashley, A. Agrawal, J. Cronin, J. Tonazzi, T.M. McCleskey, A.K. Burrell, D.S. Ehler, Anal. Chim. Acta 584 (2007) 281–286.
[7] L.A. Saari, W.R. Seitz, Analyst 109 (1984) 655–657.
[8] C. Sun, J. Wang, W. Hu, T. Xie, W. Jin, Anal. Chim. Acta 259 (1992) 319–323.
[9] M.R. Ganjali, M. Ghorbani, P. Norouzi, A. Daftari, M. Faal-Rastegar, A. Moghimi, Sens. Actuators B 100 (2004) 315–319.
[10] M.R. Ganjali, M. Rahimi-Nasrabadi, B. Maddah, A. Moghimi, M. Faal-Rastegar, S. Borhany, M. Namazian, Talanta 63 (2004) 899–906.
[11] H. Hoshino, T. Nomura, K. Nakano, T. Yotsuyanagi, Anal. Chem. 68 (1996) 1960–1965.
[12] K. Komatsu, Y. Urano, H. Kojima, T. Nagano, J. Am. Chem. Soc. 129 (2007) 13447–13454.
[13] Q. He, E.W. Miller, A.P. Wong, C.J. Chang, J. Am. Chem. Soc. 128 (2006) 9316–9317.
[14] S. Yoon, A.E. Albers, A.P. Wong, C.J. Chang, J. Am. Chem. Soc. 127 (2005) 16030–16031.
[15] A.P. de Silva, H.Q.N. Gunaratne, T. Gunnlaugsson, A.J.M. Huxley, C.P. McCoy, J.T. Rademacher, T.E. Rice, Chem. Rev. 97 (1997) 1515–1566.
[16] E.M. Nolan, S.J. Lippard, J. Mater. Chem. 15 (2005) 2778–2783.
[17] T. Gunnlaugsson, T.C. Lee, R. Parkesh, Org. Lett. 5 (2003) 4065–4068.
[18] Y. Kubo, M. Yamamoto, M. Ikeda, M. Takeuchi, S. Shinkai, S. Yamaguchi, K. Tamao, Angew. Chem. Int. Ed. 42 (2003) 2036–2040.
[19] J. Raker, T.E. Glass, J. Org. Chem. 67 (2002) 6113–6116.
[20] H. Fu, B.H. Loo, D. Xiao, R. Xie, X. Ji, J. Yao, B. Zhang, L. Zhang, Angew. Chem. Int. Ed. 41 (2002) 962–965.
[21] G.J. Mohr, I. Klimant, U.E. Spichiger, O. Wolfbeis, Anal. Chem. 73 (2001) 1053–1056.
[22] J.V. Mello, N.S. Finney, Angew. Chem. Int. Ed. 40 (2001) 1536–1538.

[23] H. Takakusa, K. Kikuchi, Y. Urano, S. Sakamoto, K. Yamaguchi, T. Nagano, J. Am. Chem. Soc. 124 (2002) 1653–1657.
[24] W.Y. Lin, L.L. Long, L. Yuan, Z.M. Cao, J.B. Feng, Anal. Chim. Acta 634 (2009) 262–266.
[25] J. Du, S.J. Yao, W.R. Seitz, N.E. Bencivenga, J.O. Massing, R.P. Planalp, R.K. Jackson, D.P. Kennedy, S.C. Burdette, Analyst 136 (2011) 5006–5011.
[26] M. Taki, J.L. Wolford, T.V. O'Halloran, J. Am. Chem. Soc. 126 (2004) 712–713.
[27] S. Maruyama, K. Kikuchi, T. Hirano, Y. Urano, T. Nagano, J. Am. Chem. Soc. 124 (2002) 10650–10651.
[28] S.C. Burdette, S. Lippard, Inorg. Chem. 41 (2002) 6816–6823.
[29] R. Yang, K. Li, K. Wang, F. Zhao, N. Li, F. Liu, Anal. Chem. 75 (2003) 612–621.
[30] Z.F. Li, Y. Xiang, A.J. Tong, Anal. Chim. Acta 619 (2008) 75–80.
[31] R.H. Yang, W.H. Chan, A.W.M. Lee, P.F. Xia, H.K. Zhang, K. Li, J. Am. Chem. Soc. 125 (2003) 2884–2885.
[32] J. Paker, T.E. Glass, J. Org. Chem. 66 (2001) 6505–6512.
[33] H. Tong, L.X. Wang, X.B. Ting, F. Wang, Macromolecules 35 (2002) 7169–7171.
[34] S. Deo, H.A. Godwin, J. Am. Chem. Soc. 122 (2000) 174–175.
[35] R. Métivier, I. Leray, B. Valeur, Chem. Commun. 8 (2003) 996–997.
[36] L. Latterini, M. Nocchetti, G.G. Aloisi, U. Costantino, F. Elisei, Inorg. Chim. Acta 360 (2007) 728–740.
[37] J. Bauer, P. Behrens, M. Speckbacher, H. Langhals, Adv. Funct. Mater. 13 (2003) 241–248.
[38] P.L. Gentili, U. Costantino, R. Vivani, L. Latterini, M. Nocchettib, G.G. Aloisi, J. Mater. Chem. 14 (2004) 1656–1662.
[39] H.P. Cong, S.H. Yu, Adv. Funct. Mater. 17 (2007) 1814–1820.
[40] H. Kakiuchida, M. Takahashi, Y. Tokuda, T. Yoko, Adv. Funct. Mater. 19 (2009) 2569–2576.
[41] G.R. Williams, D. O'Hare, J. Mater. Chem. 16 (2006) 3065–3074.
[42] F. Leroux, P. Aranda, J.P. Besse, E. Ruiz-Hitzky, Eur. J. Inorg. Chem. 6 (2003) 1242–1251.
[43] B. Sels, D. De Vos, M. Buntinx, F. Pierard, K.D. Mesmaeker, P. Jacobs, Nature 400 (1999) 855–857.
[44] A.M. Fogg, V.M. Green, H.G. Harvey, D. O'Hare, Adv. Mater. 11 (1999) 1466–1469.
[45] A.M. Fogg, J.S. Dunn, S.G. Shyu, D.R. Cary, D. O'Hare, Chem. Mater. 10 (1998) 351–355.
[46] A.I. Khan, A.J. Norquist, D. O'Hare, Chem. Commun. 22 (2001) 2342–2343.
[47] Q. Yuan, M. Wei, D.G. Evans, X. Duan, J. Phys. Chem. B 108 (2004) 12381–12387.
[48] F. Leroux, J. Gachon, J.P. Besse, J. Solid State Chem. 177 (2004) 245–250.
[49] W.Y. Shi, M. Wei, D.G. Evans, X. Duan, J. Mater. Chem. 20 (2010) 3901–3909.
[50] Z.Y. Sun, L. Jin, S.T. Zhang, W.Y. Shi, M. Pu, M. Wei, D.G. Evans, X. Duan, Anal. Chim. Acta 702 (2011) 95–101.
[51] Y.Q. Zhu, L. Zhang, J.Y. Li, Analyst 107 (1982) 957–960.
[52] Q.X. Chu, Y.Q. Zhu, Anal. Chim. Acta 149 (1983) 375–378.
[53] Y.J. Xu, X.G. Chen, Z.D. Hu, Talanta 40 (1993) 883–889.
[54] L.J. Dong, R.P. Jia, Q.F. Li, X.G. Chen, Z.D. Hu, Analyst 126 (2001) 707–711.
[55] P.P. Bontchev, S. Liu, J.L. Krumhansl, J. Voigt, Chem. Mater. 15 (2003) 3669–3675.
[56] K. Fujii, N. Iyi, R. Sasai, S. Hayashi, Chem. Mater. 20 (2008) 2994–3002.
[57] W.Y. Shi, Z.Y. Sun, M. Wei, D.G. Evans, X. Duan, J. Phys. Chem. C 114 (2010) 21070–21076.
[58] D.P. Yan, J. Lu, M. Wei, D.G. Evans, X. Duan, J. Mater. Chem. 21 (2011) 13128–13139.
[59] United States Environmental Protection Agency, Basic Information about Beryllium in Drinking Water. http://water.epa.gov/drink/contaminants/basicinformation/beryllium.cfm#water (accessed 26.01.12).
[60] H. Matsumiya, H. Hoshino, Anal. Chem. 75 (2003) 413–419.
[61] R.E. Mesmer, C.F. Baes, Inorg. Chem. 8 (1969) 618–626.
[62] G.X. Zhang, S.H. Sun, D.Q. Yang, J.P. Dodelet, E. Sacher, Carbon 46 (2008) 196–205.
[63] B. Valeur, Molecular Fluorescence: Principles and Applications, Wiley-VCH, Weinheim, Germany, 2001, p. 131.